Chapter 2
The Necessity of Sensor Calibration for the Precise Measurement of Water Fluxes in Forest Ecosystems

Shin'ichi Iida, Takanori Shimizu, Yoshinori Shinohara, Shin'ichi Takeuchi, and Tomo'omi Kumagai

2.1 Introduction

The amount of runoff from a forested watershed changes depending on the degree of tree removal (e.g., Bosch and Hewlett 1982). The forest ecosystem can greatly influence the water balance in a watershed, which, at the annual time scale, may be expressed as:

$$P = E + Q_R \tag{2.1}$$

where P is precipitation, E is evapotranspiration, and Q_R represents runoff. Evapotranspiration may be further subdivided into three components:

$$E = E_T + E_I + E_F \tag{2.2}$$

where E_T is transpiration from forest ecosystem, E_I is interception loss, and E_F is evaporation from forest floor.

As Oki and Kanae (2006) state, water resources engineers consider $P - E$ as a measure of the maximum renewable freshwater resources for a watershed (blue water). Thus, the accurate measurement of P and E, with the latter being mostly

S. Iida (✉)
Department of Disaster Prevention, Meteorology and Hydrology, Forestry and Forest Products Research Institute, Tsukuba, Ibaraki, Japan
e-mail: iishin@ffpri.affrc.go.jp

T. Shimizu
Forestry and Forest Products Research Institute, Tsukuba, Ibaraki, Japan

Y. Shinohara
University of Miyazaki, Miyazaki, Miyazaki, Japan

S. Takeuchi
Tokai University, Shizuoka, Shizuoka, Japan

T. Kumagai
University of Tokyo, Bunkyoku, Tokyo, Japan

D. F. Levia et al. (eds.), *Forest-Water Interactions*, Ecological Studies 240,
https://doi.org/10.1007/978-3-030-26086-6_2

comprised of E_T and E_I for closed-canopy forests (e.g., Wilson et al. 2001), is critical for estimating runoff generation in forest ecosystems.

Interception loss, E_I, is usually estimated as the difference between rain falling on the forest canopy and the proportion of that rain delivered to the forest floor (Helvey and Partic 1965; Carlyle-Moses and Gash 2011). Rain depth is usually measured using a tipping-bucket rain gauge or some type of tipping-bucket flow meter (e.g., Reid and Lewis 2009). However, tipping-bucket rain gauges and flow meters commonly underestimate inflow rates, especially for higher intensity rains and flow inputs (e.g., Edwards et al. 1974; Iida et al. 2018; Shimizu et al. 2018), and, as a consequence, a minimum 10% uncertainty in E_I estimates should be expected when uncorrected gauge and flow meter data are used (Iida et al. 2012). Transpiration, E_T, is evaluated using sap flow measurements with sensors inserted into the boles of trees (e.g., Kumagai et al. 2014); however, this technique may underestimate sap flux densities. For example, Steppe et al. (2010) determined that laboratory-derived sap flux densities and thus, by extension, transpiration rates of freshly cut stem segments of *Fagus grandifolia* trees were underestimated by 60%. In order to evaluate E_I and E_T correctly, the measurement uncertainties associated with tipping-bucket gauges and flow meters, as well as sap flow sensors, must be defined and taken into consideration when performing instrument calibration.

In this chapter, we describe in detail how to calibrate tipping-bucket rain gauges, tipping-bucket flow meters, and sap flow sensors (Fig. 2.1). Additionally, based on laboratory calibrations, we evaluate the effect of applying calibration on E_I estimates. Tree-to-tree and site-specific differences in calibration results of sap flow sensors and the degree of uncertainty that can be expected in estimating E_T are also evaluated and discussed.

2.2 Correction of Tipping-Bucket Rain Gauges and Flow Meters for Interception Loss Estimates

When rain falls on a forest, a proportion of the rain is stored on the tree canopies and boles that comprise some of this storage being evaporated back to the atmosphere. This interception loss (E_I) can be appreciable, accounting for 10–50% of precipitation (Roth et al. 2007). Although some researchers evaluate E_I based on the estimation of rainwater stored on the tree by detecting stem compression (e.g., Friesen et al. 2008) or a much more promising method of detecting shifts of tree sway frequency using accelerometers (e.g., van Emmerik et al. 2017; see Chap. 6 of this volume), E_I in forests is more as commonly estimated as (e.g., Carlyle-Moses et al. 2018):

$$E_I = P - (T_f + S_f) \tag{2.3}$$

where T_f is throughfall and S_f is stemflow.

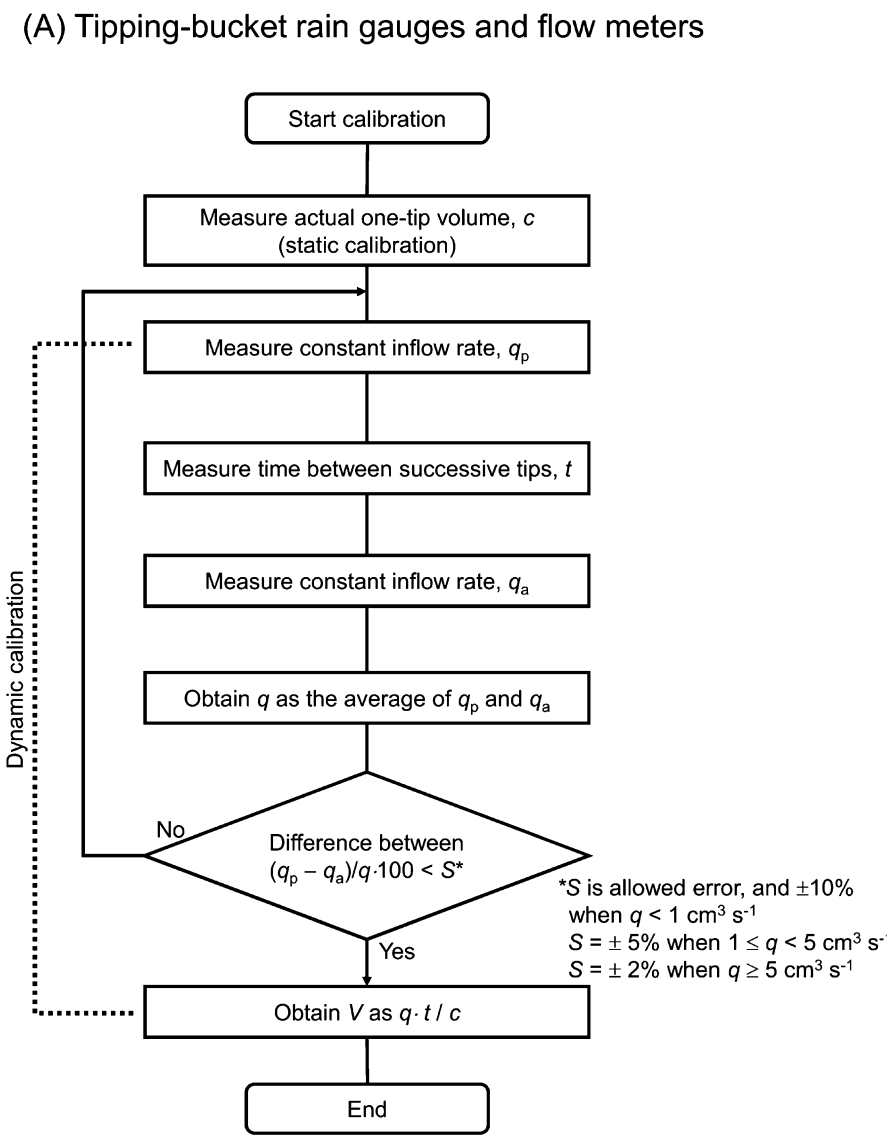

Fig. 2.1 Calibration procedures for (**a**) tipping-bucket rain gauges and flow meters and (**b**, continued on the following page) three sap flow techniques of thermal dissipation (TD) method, heat field deformation (HFD) method, and heat ratio (HR) method

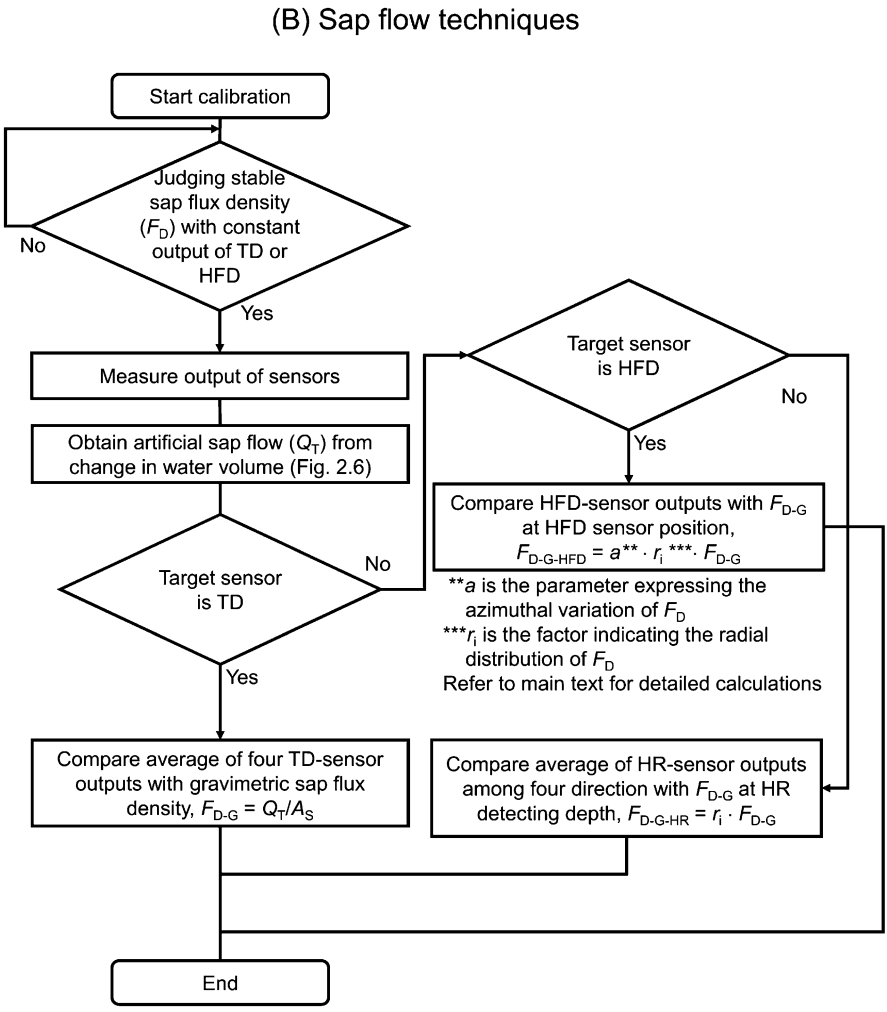

Fig. 2.1 (continued)

It is well known that T_f commonly exhibits high spatial heterogeneity with some areas of the forest floor receiving T_f inputs greater than P (e.g., Lloyd and Marques 1988; Carlyle-Moses and Lishman 2015). In order to obtain spatially representative T_f measurements, large numbers of gauges and/or gauges designed for integrating the spatial variability of T_f (e.g., trough-style gauge) are required (Carlyle-Moses et al. 2014; Su et al. 2016). Iida (2009), for example, found that for precise estimates of T_f (error $\leq$ 5%) more than 1 m^2 of gauge collection area must be distributed beneath the forest canopy of interest. Thus, the heterogeneity associated with forest overstory and the associated water routing through the canopy mean that meeting the

statistical objectives of a T_f measurement campaign will often require many more gauges than that required to estimate precipitation (e.g., Kimmins 1973; Carlyle-Moses et al. 2004; Ziegler et al. 2009). The minimum number of gauges required to estimate T_f for a desired error (ε) and confidence level (t) may be estimated using the following (Kimmins 1973; Puckett 1991):

$$n' = \frac{t^2 \cdot CV^2}{\varepsilon^2} \tag{2.4}$$

where n' is the estimated number of gauges required to sample T_f and CV is the coefficient of variation (%) of T_f measurements.

Stemflow represents water that is routed by the tree canopy to the bole where it then flows to the forest floor. Like T_f, S_f can be highly spatially variable at the plot scale since S_f yields can vary greatly among and within tree species due to factors such as tree age, canopy structure, and canopy rain shadows (Levia and Germer 2015). The quantitative importance of S_f at the individual tree scale may be expressed using the funneling ratio (Herwitz 1985) and at the forest-scale using the stand-scale funneling ratio (Levia and Gemer 2015; Carlyle-Moses et al. 2018). The funneling ratio represents the ratio of the S_f volume generated by a tree or trees to the volume of rain that would have been captured by a rain gauge having a diameter equal to that of the tree bole(s) at breast height (DBH). Funneling ratios at both the tree and forest stand-scale are often much greater than unity (e.g., Levia and Germer 2015; Carlyle-Moses et al. 2018), indicating that S_f volume is often much more than P at basal area scale. Thus, in order to obtain reasonable estimates of T_f and S_f, and therefore E_I, highly variable and often voluminous water inputs need to be measured with a high degree of accuracy.

Rainfall event scale E_I is commonly estimated based on event-scale measurements of P, T_f, and S_f (e.g., van Dijk et al. 2015), employing storage-type gauges and large-capacity collection reservoirs. However, for a better understanding of the interception process, including the impact of meteorological factors and tree characteristics, more work examining the dynamics of E_I is necessary at the intra-event time scale using high temporal resolution T_f and S_f measurements by tipping-bucket rain gauges and flow meters (e.g., Reid and Lewis 2009; Iida et al. 2017) as well as instrument systems utilizing ultrasonic rangefinders to monitor changes in collected flow depths (Turner et al. 2019). In such cases, the well-known systematic biases of tipping-bucket rain gauges and flow meters must be considered. When the bucket mechanism of a tipping-bucket gauge or flow meter is filled with water, it tips the other bucket into position to continue receiving water input. The water flux is then measured as the number of tips over a duration with this information being stored on a datalogger. If, however, water flows continuously during the period between one bucket tipping and the other bucket being brought into position, a certain amount of water does not flow into either bucket and is not registered with the degree of water input underestimation increasing with increasing intensity of inflow. This systematic underestimation has been reported and dynamically calibrated (e.g., Edwards et al. 1974). Moreover, the static amount of a tip (c), which is the volume

Table 2.1 A list of calibration curves for various tipping-bucket rain gauges and flow meters

Type	One tip volume (c_m, mL)	Calibration curve		Source
Tipping-bucket rain gauge (TBRG)				
OC[a]	3.73	$V = -0.0352Q^2 + 0.418Q + 1$	$R^2 = 0.99$	Iida et al. (2012)
OT[b]	15.7	$V = -0.119Q^2 + 0.454Q + 1$	$R^2 = 0.97$	Iida et al. (2012)
DI[c]	4.28	$V = -0.2005Q^2 + 0.702Q + 1$	$R^2 = 0.95$	Iida et al. (2018)
Tipping-bucket flow meter (TBFM)				
U50[d]	50	$V = -0.189Q^2 + 0.531Q + 1$	$R^2 = 0.99$	This study
U100[e]	100	$V = -0.906Q^2 + 0.971Q + 1$	$R^2 = 0.96$	This study
U200[f]	200	$V = -0.492Q^2 + 0.719Q + 1$	$R^2 = 0.98$	Iida et al. (2012)
U200[f]	200	$V = -0.489Q^2 + 0.672Q + 1$	$R^2 = 0.85$	Shimizu et al. (2018)
U500[g]	500	$V = -0.632Q^2 + 0.814Q + 1$	$R^2 = 0.98$	This study
I200[h]	200	$V = -0.161Q^2 + 0.554Q + 1$	$R^2 = 0.98$	Iida et al. (2012)
I400[i]	400	$V = -0.756Q^2 + 0.719Q + 1$	$R^2 = 0.95$	Iida et al. (2012)
Y500[j]	500	$V = -0.258Q^2 + 0.907Q + 1$	$R^2 = 0.97$	Shimizu et al. (2018)

[a]RG-3 M, Onset Computer Corp., Massachusetts
[b]OW-34-BP, Ota keiki seisakusho Co., Ltd., Tokyo, Japan
[c]Rain Collector II, Davis Instruments, California
[d]UIZ-TB-50, Uizin Co., Ltd, Tokyo., Japan
[e]UIZ-TB-100, Uizin Co., Ltd, Tokyo., Japan
[f]UIZ-TB-200, Uizin Co., Ltd, Tokyo., Japan
[g]UIZ-TB-500, Uizin Co., Ltd, Tokyo., Japan
[h]TXQ-200, Ikeda keiki seisakusho Co., Ltd., Tokyo, Japan
[i]TXQ-400, Ikeda keiki seisakusho Co., Ltd., Tokyo, Japan
[j]500 mL model Yokogawa Electric Corp., Tokyo, Japan

associated with one tip of the tipping-bucket mechanism under very low intensity inflows, is frequently found to be different from that stipulated by the gauge or flow meter manufacturer (c_m) (Shedekar et al. 2016; Iida et al. 2018; Shimizu et al. 2018). Thus, static calibration is critical for measuring water fluxes correctly with tipping-bucket rain gauges and flow meters. The necessary calibrations for several tipping-bucket and flow meter models have been reported (Iida et al. 2012, 2018; Shimizu et al. 2018; see Table 2.1). Based on these results and the established need to correct for the under-catch of these gauges and flow meters, we explain and detail the procedure necessary to properly calibrate these instruments.

2.2.1 Static Calibration Methods

The calibration results of three tipping-bucket rain gauge models and eight tipping-bucket flow meter models amalgamated from the existing literature and this study are presented in Table 2.1. At first, static calibration, which quantifies the volume of one

tip (c) directly, should be conducted (Fig. 2.1). Once c has been established, the relationship between the inflow rate and the actual amount one tip is determined by dynamic calibration.

Since manufacture stated tip-inducing volumes (c_m) for the tipping-bucket rain gauges are all <16 mL (Table 2.1), we used injectors to fill the tipping-bucket mechanism with water on a drop by drop basis in order to obtain the volume of water required to cause a single tip (c). More specifically, c was found as the difference in the mass, using an electronic scale, of the injector plus the water within the injector at the start of the calibration procedure and the mass of the injector plus the water remaining in the injector once a tip had occurred. However, tipping-bucket flow meters have stated c_m values > 50 mL and, in order to avoid injection errors while determining c for these instruments, a beaker was used to help facilitate the calibration procedure. When calibrating the U50 flow meter, for example, 40-mL of water was initially added to the bucket with the injector being used for subsequent additions of water until c was realized.

2.2.2 *Dynamic Calibration Methods*

For dynamic calibration, it is imperative that a constant inflow rate (q, mL s^{-1}) be obtained. The key to maintain a stable q during the calibration procedure is to keep a constant difference in head between the inlet and outlet of water flow. A simple apparatus, depicted in Fig. 2.2, is used to generate q. The constant difference in head can be attained by maintaining an overflow of water (Fig. 2.2). The value of q is given as the mass of stored water, measured by an electronic balance, over a certain duration determined by a stopwatch. For each intensity of q, at least 10 tips are

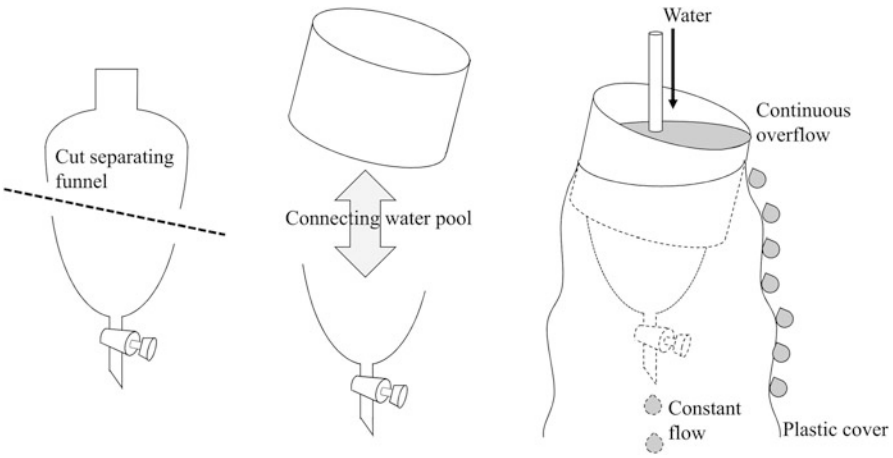

Fig. 2.2 Simple instrument to generate constant water flow for tipping-bucket rain gauge and flow meter calibrations

recorded as the times of each tip with 10 Hz with a datalogger (type CR1000, Campbell Scientific Inc., Logan, Utah). The average time between tips (t, s) is derived, while the volume associated with a tip (v, mL) is found as:

$$v = q \cdot t. \tag{2.5}$$

Constant inflow-volume relationships may vary even for the same type of tipping-bucket rain gauge or flow meter model. Shiraki and Yamato (2004) proposed that a common relationship for the same model of gauge or flow meter can be obtained by scaling q and v with c, with $Q = q/c$ and $V = v/c$. The best fit of the $Q - V$ relationships for all tipping-bucket rain gauges and flow meters evaluated is a quadratic curve (Table 2.1).

$$V = d \cdot Q^2 + e \cdot Q + 1 \tag{2.6}$$

where d and e are the fitting parameters.

As aforementioned, the underlying cause of the underestimation in water input rates is the failure of capturing q during the time of the tip (Δt). If Δt is constant to Q, the $Q - V$ relationship must be fitted with a linear equation ($V = \Delta t \cdot Q + 1$). However, since a quadratic curve has been found to be a better fit of the Q-V relationship and not the linear line, this implies that Δt decreases with increasing Q (Iida et al. 2012). Shiraki et al. (2018) measured Δt by high-speed-digital video, and confirmed the decreasing trend in Δt with increasing Q. Shiraki et al. (2018) also noted that the movement of stored water resulting from the high kinetic energy of Q, decreases the value of V compared with the predicted value from a linear relationship derived using a smaller range of Q.

Constant inflow, Q, can be obtained from Eq. 2.6 and that V can be equated with $Q \cdot t$:

$$Q = \frac{-(e - t) - \sqrt{(e - t)^2 - 4d}}{2d} \tag{2.7}$$

For the application of the calibration curves to data obtained in the field, Q is first calculated by substituting t into Eq.2.7, while the volume associated with a single tip is obtained as the product of c, Q, and t (Eq. 2.5), that is, $v = q \cdot t = c \cdot Q \cdot t$.

2.2.3 *Dynamic Calibration of Tipping-Bucket Rain Gauges and Flow Meters*

Of all the tipping-bucket rain gauges and flow meters evaluated, the U100 tipping-bucket flow meter shows the most significant underestimation of V for smaller values of Q (Table 2.1, Fig. 2.3). For this model, a 10% underestimation of V (i.e., $V = v/c = 1.1$) occurs when $Q > 0.12\ \mathrm{s}^{-1}$. For tipping-bucket rain gauges,

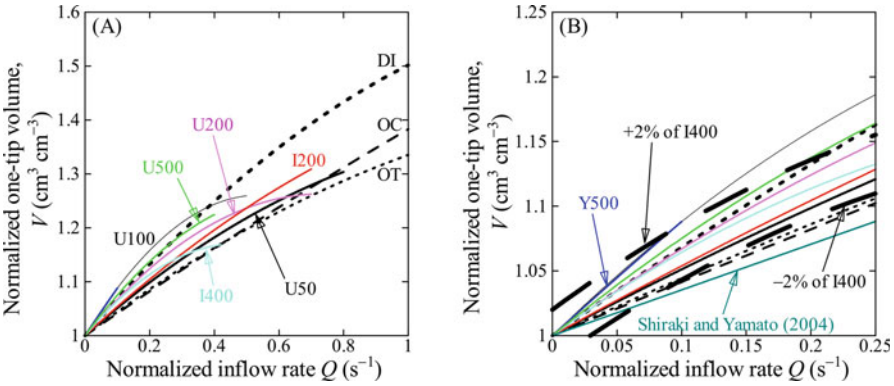

Fig. 2.3 Relationships between normalized inflow rate (Q) and one-tip volume (V) for a range of Q from (**a**) 0 to 1 and (**b**) 0 to 0.25 s^{-1}. Refer to Table 2.1 for details of target tipping-bucket rain gauges and flow meters and calibration curves

the OT and OC models have a relatively small amount of underestimation, and 10% errors are not detected for Q values less than 0.24 s^{-1} (Fig. 2.3). If U100 has $c = 100$ mL and $Q = 0.12$ s^{-1} then q ($q = c \cdot Q$) is 12 mL s^{-1}. Additionally, if the c of the OT and OC rain gauges are 0.5 and 0.2 mm, respectively, then $Q = 0.24$ s^{-1} and thus $q = 0.12$ mm s^{-1} and 0.048 mm s^{-1}, respectively.

For almost all types of large tipping-bucket flow meters ($c_m \geq$ 150–200 mL), Shimizu et al. (2018) suggest that the $Q - V$ relationships obtained through laboratory tests can be plotted within the range of ±2% of that for the I400 model (Table 2.1) when Q is less than 0.1–0.2 s^{-1} (corresponding to 0.1–0.2 Hz tipping rate). This indicates the calibration equation for I400 can be applicable for most types of large tipping-bucket flow meters. However, our calibration results for the U100 model found that the $Q - V$ relationship exceeds the +2% range of the I400 gauge when $Q \geq 0.1$ s^{-1} (Fig. 2.3b). Considering that a high frequency tip rate occurs more readily on a tipping-bucket flow meter with a relatively small c_m, precaution must be taken when applying the equation for the I400 flow meter to flow meters with $c_m \leq 100$ mL.

Similar to the U100 gauge, the $Q - V$ relationships for the OT and OC tipping-bucket rain gauges lie outside of the −2% range of the I400 flow meter even when $Q \approx 0.1$ s^{-1} or less (Fig. 2.3b). The DI rain gauge (Table 2.1), however, was found to have a $Q - V$ relationship that was within the +2% range when $Q < 0.22$ (Fig. 2.3b). These findings suggest the difficulty in establishing a representative dynamic calibration equation which would cover most tipping-bucket rain gauges. Shiraki and Yamato (2004) proposed a common calibration eq. ($V = 0.353Q + 1$) for tipping-bucket rain gauges; however, it should be noted that the equation lies within the lowermost of the plots in Fig. 2.3b. As such, the application of the Shiraki and Yamato (2004) equation underestimates the water input for all tipping-bucket rain gauges. Determining if a common calibration equation that could be applied to most types of tipping-bucket rain gauges can be derived should be revisited once laboratory and field tests for larger samples of several of tipping-bucket rain gauges and flow meters has been accomplished.

2.2.4 Cautions for Applying the Calibration to Measured Data

Applying static calibration to tipping-bucket rain gauges and flow meters is critical to measure q correctly. Shimizu et al. (2018) reported a maximum difference between c and c_m of +2.5% for larger tipping-bucket flow meters. Maximum differences between c and c_m among the tipping-bucket rain gauges and 200-mL flow meters calibrated by Iida et al. (2012) were −15% and +3.2%, respectively. Additionally, Iida et al. (2018) found that the difference between c and c_m was −16% for the DI-type tipping-bucket rain gauge. These examples clearly illustrate the need for the static calibration of all types of tipping-bucket rain gauges and flow meters.

High-frequency data (e.g., 10 Hz) were used for the dynamic calibrations of the tipping-bucket rain gauges and flow meters. However, field measurements are usually recorded as the accumulated number of tips, n_t, during a given duration, D. In these circumstances, instead of actual t, the average time between tipping T, found as $T = D/n_t$, is substituted into (Eq. 2.7) and the corrected v is derived. However, if D is longer than a suitable range, T can be overestimated and the degree of correction to v would be smaller than that based using actual t. Iida et al. (2012) investigated the suitable range of D for a temperate forest in Japan and a tropical forest in Cambodia. The D values obtained were up to 60 min and 10 min for P and T_f measurements in the temperate and the tropical forest, respectively. Stemflow measurements required $D < 150$ s for a tree having a DBH of 25.5 cm and funneling ratios > 10 in the tropical forest, while in the temperate forest $D = 600$ s was suitable for a tree with a DBH of 27.1 cm and funneling ratios < 20 (Iida et al. 2012). However, these examples of D may not be applicable to measurements of P, T_f and S_f for different forest ecosystems. As such, we recommend that D be set to the shortest time interval permissible based on the measurements of t for interception studies.

2.2.5 Effect of Dynamic Calibration on Interception Loss Estimates

Interception loss (E_I) is calculated as the difference between P and the sum of T_f and S_f (see Eq. 2.3). P is the largest component of (Eq. 2.3), and therefore, in most cases, the amount of correction by dynamic calibration is largest for P. Thus, if the dynamic calibration is not applied, E_I would be underestimated. However, there are some cases that E_I is overestimated for combinations of different types of tipping-bucket rain gauges (Fig. 2.4, Iida et al. 2018). We investigated the nine combinations of P and T_f measurements with three tipping-bucket rain gauge models (type OT, OC, and DI; Table 2.1). When the same model of tipping-bucket rain gauge is used to measure both P and T_f, the effects on E_I are relatively small (Fig. 2.4a, b, and c). The

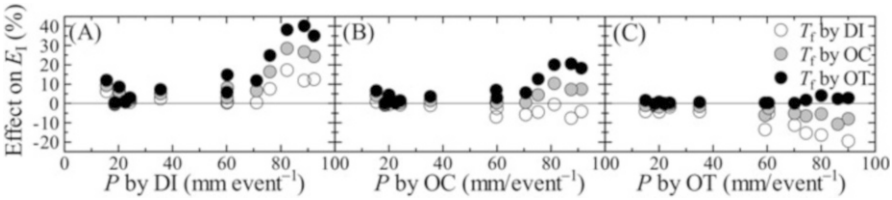

Fig. 2.4 Effect of dynamic calibrated gross rainfall (P) and throughfall (T_f) on interception loss (E_I). (**a**) P is measured by Rain Collector II, Davis Instruments (DI), (**b**) RG-3M, Onset Computer Corp. (OC), and (**c**) OW-34-BP, Ota keiki seisakusho Co., Ltd. (OT). 10% effect means 10% increase in E_I after applying the correction, that is, 10% underestimation. Data are cited from Iida et al. (2018)

best scenario is the combination of both P and T_f measured with the OT gauge, in which a maximum effect on E_I of +4% is detected (Fig. 2.4c). A +4% error, however, is not negligible, and thus, even under optimum conditions, tipping-bucket gauges require correction using the dynamic calibration curve. The fact that evaluation of spatially representative T_f needs many tipping-bucket rain gauges, it can be expected that lower-cost tipping-bucket rain gauges, such as the DI type, would be used for T_f measurements. However, a −20% error in E_I (20% overestimation) is found when T_f is measured with the type DI gauge (Fig. 2.4c), having the largest systematic bias among the three tipping-bucket rain gauges evaluated (Fig. 2.3a). If the DI-type tipping-bucket rain gauge is also used to measure P, E_I is underestimated by as much as 40% (Fig. 2.4a).

This section discussed the error associated with tipping-bucket rain gauges and flow meters at the rainfall-event scale. If, however, the dynamics of the interception process during the rainfall event are to be investigated (Reid and Lewis 2009, Iida et al. 2017), then dynamic calibrations at the hourly time scale are highly recommended.

2.3 Calibration of Sap Flow Sensors Measuring Forest Transpiration

Sap flux density, F_D, measurements are widely used to evaluate forest transpiration, E_T (Wilson et al. 2001; Kumagai et al. 2008; Oishi et al. 2008). Transpiration from a tree, using sap flow (Q_T) as a surrogate, can be estimated as the product of sapwood area (A_S) and F_D averaged over sapwood area, $\overline{F_D}$:

$$Q_T = A_S \cdot \overline{F_D}. \tag{2.8}$$

Transpiration can be estimated by scaling Q_T up from the tree to the stand level (e.g., Kumagai et al. 2008). Both A_S and $\overline{F_D}$ are required in order to estimate E_T, and

a detailed analysis is necessary to derive the number of samples required to estimate the representative values of A_S and $\overline{F_D}$ (Kumagai et al. 2005a, b).

The focus of this section is on the required calibration associated with three different sap flow techniques, namely, (i) thermal dissipation (TD) (Granier 1985), (ii) heat ratio (HR) (Burgess et al. 2001), and (iii) heat field deformation (HFD) (Nadezhdina et al. 2012) (Figs. 2.1 and 2.5a). All three techniques insert probes and a heater into a stem and detect the F_D by using heat as a tracer. Recently, some studies report that TD underestimates F_D (e.g., Steppe et al. 2010; Peters et al. 2018) and uncertainties of measuring F_D with HFD (e.g., Steppe et al. 2010; Fuchs et al. 2017). We sampled stem segments of Japanese cedar (*Cryptomeria japonica*) planted in the nursery of the Forestry and Forest Products Research Institute (FFPRI), Tsukuba, approximately 50 km northeast of Tokyo, and in the Nagasaka Experimental Watershed, northern Honshu island (Table 2.2). An artificial Q_T is

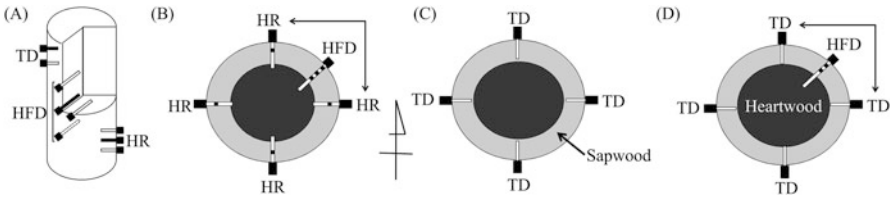

Fig. 2.5 Schematic diagram showing (**a**) sap flow sensors of three methods of thermal dissipation (TD), heat field deformation (HFD), and heat ratio (HR) and (**b**, **c**, **d**) arrangements of sensors used in calibration. Black colored probe includes heater. Arrangements of sensors for tree segments of (**b**) F1 to F4, (**c**) F5 to F8, and (**d**) N1 to N5 are indicated (refer to Table 2.2). Note that the measurement points are marked as black squares for sensors of HFD and HR methods (**b** and **d**). Sensors indicated by arrows are used to calculate the coefficient of *a* (**b** and **d**)

Table 2.2 Characteristics of the Japanese cedar test trees

Segment	DBH (cm)	TH (m)	*SW* (cm)	A_S (cm^2)	Calibration
FFPRI nursery					
F1	11.1	9.7	3.6	78.6	HR, HFD
F2	10.9	9.0	2.8	68.1	HR, HFD
F3	12.2	10.0	3.0	81.1	HR, HFD
F4	12.5	9.1	3.1	86.2	HR, HFD
F5	11.6	9.5	2.8	73.6	TD
F6	11.5	9.8	2.5	69.2	TD
F7	11.2	9.3	2.4	60.2	TD
F8	11.5	9.2	2.4	65.0	TD
Nagasaka					
N1	13.4	16.5	2.1	68.9	TD, HFD
N2	12.5	14.1	1.9	59.1	TD, HFD
N3	13.9	14.7	1.7	61.2	TD, HFD
N4	12.0	14.7	1.9	55.5	TD, HFD
N5	11.8	9.9	1.9	56.1	TD, HFD

generated by applying negative pressure at the upper surface of the segment with a vacuum pump and calibration of the three techniques was conducted in the laboratory.

2.3.1 Characteristics of the Three Sap Flow Techniques

The thermal dissipation, TD, method proposed by Granier (1985) inserts a pair of thermocouples into a plant stem (Fig. 2.5a). The upper probe measures the temperature of an included heater to generate constant heat of 0.2 W, while the lower probe measures the xylem temperature as a reference. The space between probes should be more than 10 cm (Iida and Tanaka 2010), while the length of the probes is 2.0 cm. The temperature difference between the probes (ΔT) increases during low F_D and decreases with increasing F_D. Granier (1985) obtained the following calibration curve between the parameter K_{TD} and F_D:

$$F_{D-TD} = 42.84 \cdot {K_{TD}}^{1.231} = 42.84 \cdot \left(\frac{\Delta T_0 - \Delta T}{\Delta T}\right)^{1.231} \tag{2.9}$$

where $F_{D\text{-}TD}$ is the F_D measured by the TD method ($cm^3\ cm^{-2}\ h^{-1}$), and ΔT_0 is ΔT when $F_D = 0$. We employed handmade sensors described by Kumagai et al. (2005a). The TD sensor detected the average F_D across the range of probe.

The heat field deformation (HFD) method also uses heat to measure F_D. A continuously powered heater is inserted at the center of the upper and lower temperature probes with an additional temperature probe installed tangentially next to the heater (Fig. 2.5a). F_D is calculated by the following Nadezhdina et al. (2012):

$$F_{D-HFD} = \frac{D(K_{HFD} + dT_{s-a})Z_{ax}}{dT_{as} \cdot Z_{tg} \cdot SW} \cdot 3600. \tag{2.10}$$

where $F_{D\text{-}HFD}$ is F_D measured by HFD ($cm^3\ cm^{-2}\ h^{-1}$), $dT_{s\text{-}a}$ is the temperature difference between the upper and tangential probes (°C), or can be equated with the difference between dT_{sym} and dT_{as}, which represent the temperature differences (°C) between the upper and lower probes and between the tangential and lower probes, respectively, Z_{ax} is the difference between the heater and upper or lower temperature probe (1.5 cm), Z_{tg} is the distance between the heater and the tangential probe (0.5 cm), and SW is the width of sapwood (cm), while K_{HFD} is the $dT_{s\text{-}a}$ when F_D is equal to zero.

Nadezhdina et al. (2012) found that the ratio of dT_{sym} to dT_{as} (dT_{sym}/dT_{as}) has a linear relationship with F_D and that K_{HFD} may be equated with the y-intercept value of the linear regression between dT_{sym}/dT_{as} (dependent variable) and dT_{as} (independent variable). Since the absolute value of $dT_{s\text{-}a}$ is equal to that of dT_{as} when F_D is zero, the absolute value of y-intercept derived from the linear regression between dT_{sym}/dT_{as} and $dT_{s\text{-}a}$ must be equal to that between dT_{sym}/dT_{as} and dT_{as}. The

HFD method determines K_{HFD} objectively based on two linear regressions which meet the condition of having the same absolute values of y-intercepts, representing an advantage of the HFD method (Nadezhdina et al. 2012). We used a commercial HFD sensor (HFD8, ICT international Pty. Ltd.). The length of the heater and temperature probes are 11.7 and 9.7 cm, respectively, and eight thermistors are positioned in a 1-cm span from the probes. We inserted temperature probes into tree stem segments to locate the first thermistor at the depth of 0.5 cm in sapwood.

The heat ratio, HR, method, which is an alternate version of heat pulse method, calculates heat pulse velocity (HPV_r, cm h^{-1}) based on the temperature changes of the xylem caused by induced heat by a heater and measured with two temperature probes located at the same distance from the heater (Fig. 2.5a). HPV_r is then found as (Marshall 1958; Burguess et al. 2001):

$$HPV_r = \frac{D}{x} \ln\left(\frac{v_1}{v_2}\right) \cdot 3600. \tag{2.11}$$

where D is thermal diffusivity of fresh wood (2.5×10^{-3} cm^2 s^{-1}; Marshall 1958), x is the distance between the heater and the temperature probe (0.5 cm), v_1 and v_2 are the increase of xylem temperature (°C) by heat detected by the upper and lower temperature probes, respectively.

HPV_r is affected by the wounding effect caused by the nonconducting wood around the probes, which results from the mechanical damage to the xylem tissue during sensor installation (Swanson and Whitfield 1981; Burgess et al. 2001). Burgess et al. (2001) proposed the following equation to correct for the wounding effect:

$$HPV_c = B \cdot HPV_r. \tag{2.12}$$

where HPV_c is corrected HPV_r by considering the wounding effect, B is the correction coefficient. In this study, we assume the wound width of 0.17 cm and applied a B value of 1.7283 (Burgess et al. 2001). Sap flux density, F_D, measured with the HR method ($F_{D\text{-}HR}$) is then derived as:

$$F_{D-HR} = \frac{\rho_b}{\rho_s}\left(m_c + \frac{c_{dw}}{c_s}\right) HPV_c. \tag{2.13}$$

where ρ_b is dry wood density of Japanese cedar (0.314 g cm^{-3}; Fujiwara et al. 2004), ρ_b is density of sap assumed to be equal to the density of water (1.0 g cm^{-3}), m_c is the mass of the water content of sapwood relative to dry weight of sapwood (1.78), c_{dw} is the specific heat capacity of oven-dried wood (J g^{-1} °C^{-1}), and c_s is the specific heat capacity of sap, assumed to be equal to that of water (4.186 J g^{-1} °C^{-1}).

The ratio of c_{dw} to c_s is often assumed to be constant at 0.33 (=1.380/4.186; Dunlap 1912; Edwards and Warwick 1984; Steppe et al. 2010). We used a commercial HR sensor (type SFM1, ICT international Pty. Ltd.), whose sensor length is

3.5 cm including two thermistors to detect v at different depths. We installed sensors into stem segments to detect $F_{\text{D-HR}}$ at the depth of 1 cm of sapwood.

2.3.2 *Artificial Sap Flow Generated by a Vacuum Pump*

In order to calibrate the sap flow techniques, an artificial and known Q_T is required. Granier (1985) generated Q_T by applying positive water pressure on the tree segment. Similar methods of generating Q_T using positive pressures have also been proposed (Herbst et al. 2007; Steppe et al. 2010; Hubbard et al. 2010; Bosch et al. 2014; Fuchs et al. 2017; Ouyang et al. 2018; Peters et al. 2018). In some instances, a negative pressure has been used to control Q_T (Taneda and Sperry 2008; Bush et al. 2010; Schmidt-Walter et al. 2014). Additionally, the amount of transpiration from a tree, which equates with Q_T, has been found by monitoring the change in mass of trees planted in a lysimeter (Lu and Chako 1998; Mcculloh et al. 2007). Takeuchi et al. (2017) excavated a tree, including the root-ball—a common practice for transplanting trees—with Q_T equated to the changes in the total mass of the tree and root-ball, a technique the authors termed the "weighing root-ball" method. Sun et al. (2012) estimated Q_T using potometer experiments, in which cut foliated tree branches were submerged into water and the amount of absorbed water was measured, while Lopez et al. (In press) cut *Eucalyptus grandis* trees ranging from 3 to 6 cm in diameter and submerged them into a fixed-volume reservoir with Q_T found as the change in the volume of water held in the reservoir.

In this study, we apply negative pressure to generate Q_T within a cut stem segment of Japanese cedar (Fig. 2.6) (Shinohara et al. 2016). An attachment designed to clean the inside of the PVC pipe (Fig. 2.6) was fixed to the upper surface of the cut segment and connected to a vacuum pump. Then, the segment was

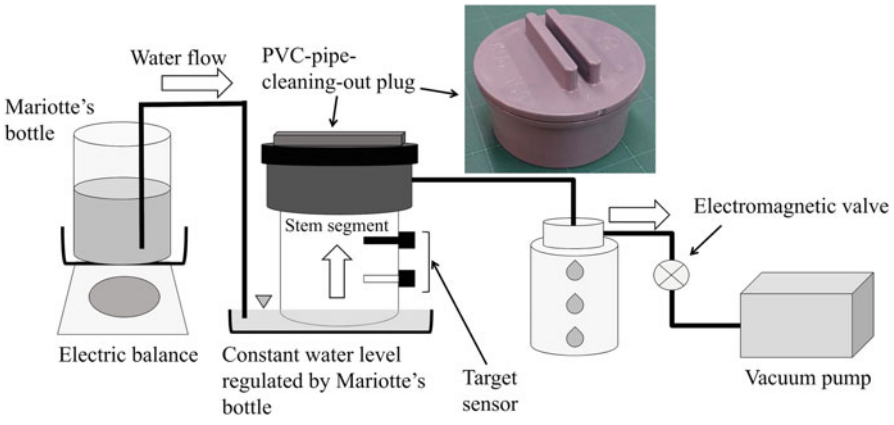

Fig. 2.6 A vacuum pump system to generate artificial sap flow within a stem segment, originally devised by Shinohara et al. (2016)

suspended by the cable ties, and its lower surface was submerged into free water surface. Depending on the pressure gradient, which was typically between 0.03 and 0.14 MPa/m, the lower surface absorbs KCl solution. This water surface was kept at a constant level with a Mariotte's bottle. The water flow, Q_T, was then found as the decrease in weight of the Mariotte's bottle with an electric balance with a 10-sec temporal resolution.

Precise calibration of the sap flow techniques is accomplished by comparing the actual F_D at the sensor position to the F_D measured by the sensor. When cut stem segments are used, the actual value of Q_T is obtained and the gravimetric sap flux density, $F_{D\text{-}G}$, is derived within a segment as Q_T/A_S (Fig. 2.1, Eq. 2.8). For each of the segments calibrated, a clear radial trend in $F_{D\text{-}HFD}$ was found (Fig. 2.7a, Table 2.2), and different $F_{D\text{-}TD}$ were measured among the four cardinal directions (i.e., north, east, south, and west) (Fig. 2.7b, Table 2.2). Similar results of radial and azimuthal distribution of the F_D within stem segments have been reported by Steppe et al. (2010). Thus, it is likely that the actual F_D derived at sensor position is not equal to $F_{D\text{-}G}$ and that the sensor output at the single position is not sufficient to perform suitable calibrations. In this study, measurements of F_D variations over sapwood area for all cut stem segments were made (Fig. 2.5b, c, d).

2.3.3 *Calibration of the TD Method*

Tree stem segments with *SW* being approximately 2.0 cm (equal to the senor length) were selected for the TD calibrations (Table 2.2). The four TD sensors were inserted into the stem segments so that the azimuthal variation of F_D (north, east, south, and

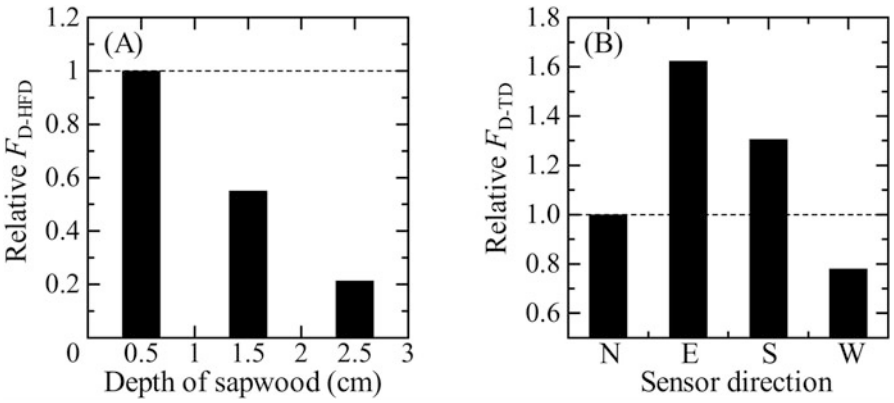

Fig. 2.7 Panel (**a**) shows radial distribution of sap flux density detected by HFD sensor ($F_{D\text{-}HFD}$) in cut segment of F4 (see Table 2.2). $F_{D\text{-}HFD}$ was shown as relative to $F_{D\text{-}HFD}$ measured at 0.5 cm depth (see Fig. 2.5B). Panel (**b**) indicates azimuthal variation in sap flux density measured by four TD sensors ($F_{D\text{-}TD}$) installed in a cut segment of N2 (see Table 2.2). North, east, south, and west $F_{D\text{-}TD}$ are shown as relative to north $F_{D\text{-}TD}$ (see Fig. 2.5d)

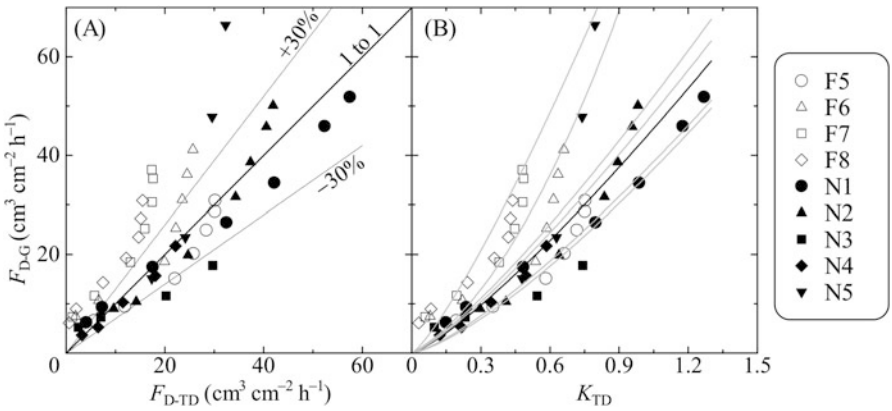

Fig. 2.8 Comparisons of gravimetric sap flux density ($F_{D\text{-}G}$) and (**a**) measured sap flux density with TD method ($F_{D\text{-}TD}$), and (**b**) parameter K_{TD}. Open and black symbols show the data measured at the segments of Japanese cedar sampled in FFPRI nursery and Nagasaka site, respectively. Black curve is the original calibration by Granier (1985), and the gray curves are previously published calibrations for softwood species (Sun et al. 2012; Bosch et al. 2014; Ouyang et al. 2018; Peters et al. 2018)

west directions) was accounted for and the averaged $F_{D\text{-}TD}$ is compared with $F_{D\text{-}G}$ (Fig. 2.1). Note that when *SW* is less than 2.0 cm, the correction proposed by Clearwater et al. (1999) should be applied. The $F_{D\text{-}TD}$ values were found to be within ±30% of the $F_{D\text{-}G}$ of stem segments sampled at Nagasaka site (Fig. 2.8a). Thus, for the Nagasaka site stem segments, clear underestimations of $F_{D\text{-}TD}$ were not found. However, for stem segments at the FFPRI nursery, most $F_{D\text{-}TD}$ values were found to be less than $F_{D\text{-}G}$ and underestimations of $F_{D\text{-}TD}$ were detected. Relatively high tree-specific variations among the $F_{D\text{-}TD}$ data were found for the four FFPRI stem segments, illustrating the difficulty of establishing a calibration equation. Almost all the variations in the relationship between the parameter K_{TD} and $F_{D\text{-}G}$ for the nine stem segments (87% of data plotted in Fig. 2.8b) are in the range of the reported calibration curves.

2.3.4 Calibration of the HFD Method

It is important to recognize that the heat field deformation, HFD, method measures point F_D at the detection depths in rather than measuring the average F_D along the TD sensor. We derived the gravimetric F_D values at the HFD sensor measurement points, $F_{D\text{-}G\text{-}HFD}$, as follows: Four FFPRI stem segments and five Nagasaka stem segments (Table 2.2) were used with F_D measured in each of the four cardinal directions with a HR sensor (Fig. 2.5b) for the FFPRI stem segments, while for the Nagasaka stem segments, four TD sensors were installed in each direction

(Fig. 2.5d). The ratio of the average of two-direction values measured by the HR or TD method to the average of all four direction values (a) was calculated (2.5b, d). The radial distribution of F_D is obtained from $F_{D\text{-}HFD}$ measurements at the different depths within the sapwood (Fig. 2.5b, d). We calculate the ratio of $F_{D\text{-}HFD}$ at a certain depth (i) to the average $F_{D\text{-}HFD}$ for all depths within the sapwood (r_i), and gravimetric sap flux density at the detection point of the HFD sensor, $F_{D\text{-}G\text{-}HFD}$, at the depth of i can be obtained as $a \cdot r_i \cdot F_{D\text{-}G}$ (Fig. 2.1).

The plots of $F_{D\text{-}HFD}$ were found to be distributed around the 1:1 relationship with $F_{D\text{-}G\text{-}HFD}$, however, relatively high dispersion of $F_{D\text{-}HFD}$ with values overlying +30% or underlying −30% was also found (Fig. 2.9a), indicating large tree-to-tree differences. Focusing on FFPRI stem segments, the HFD method clearly underestimated $F_{D\text{-}G\text{-}HFD}$ with the linear relationship of $F_{D\text{-}G\text{-}HFD} = 1.33\ F_{D\text{-}HFD}$, $R^2 = 0.72$, being derived (Fig. 2.9b). However, when the Nagasaka stem segments are considered, the values show relatively high variability and trends of overestimation or underestimation were not detected ($F_{D\text{-}G\text{-}HFD} = 0.94\ F_{D\text{-}HFD}$, $R^2 = 0.69$).

2.3.5 *Calibration of the HR Method*

The heat ratio, HR, method was calibrated using the four FFPRI stem segments (Table 2.2, Fig. 2.5b). Similar to the HFD method, the HR sensor measures point F_D. The gravimetric F_D at the detecting point of the HR sensor ($F_{D\text{-}G\text{-}HR}$) is calculated using the similar methodology as for the HFD calibrations. In this case, four-direction values of $F_{D\text{-}HR}$ were measured, and we compared the averaged $F_{D\text{-}HR}$

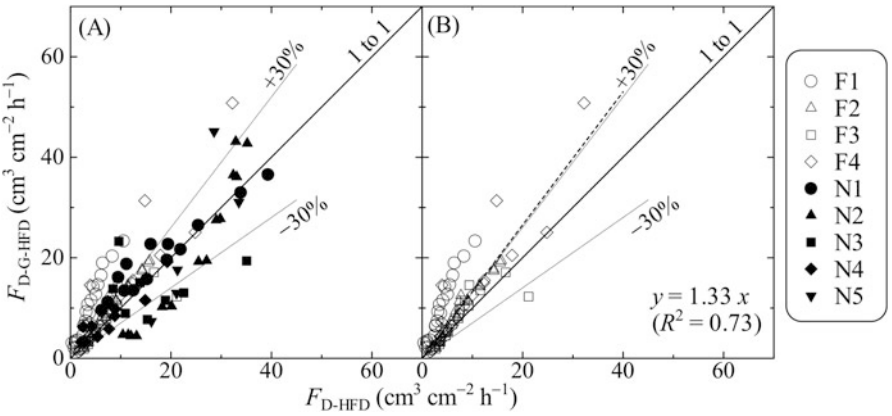

Fig. 2.9 Relationship between gravimetric sap flux density at sensor position of heat field deformation (HFD) method ($F_{D\text{-}G\text{-}HFD}$) and measured sap flux density with HFD ($F_{D\text{-}HFD}$) for (**a**) all cut segments and (**b**) FFPRI nursery segments (F1 to F4 in Table 2.2). The dashed line shows the linear regression for FFPRI stem segments ($y = 1.33x$, $R^2 = 0.72$)

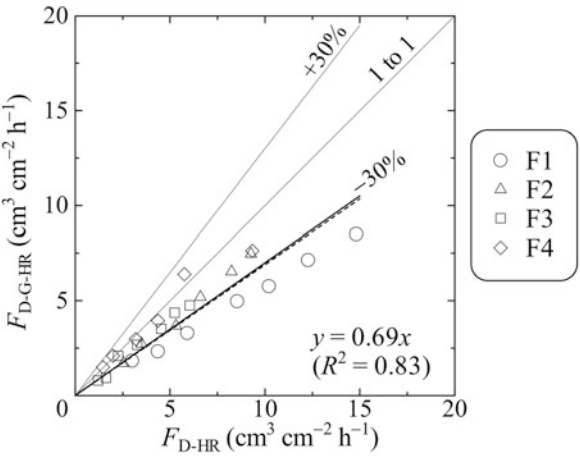

Fig. 2.10 Relationship between gravimetric sap flux density at the detecting depth of heat ratio (HR) method ($F_{\text{D-G-HR}}$) and measured sap flux density with HR ($F_{\text{D-HR}}$). The dashed line indicates the regression line ($y = 0.69x$, $R^2 = 0.83$)

values among four directions with the gravimetric sap flux density at the measuring depth of HR, $F_{\text{D-G-HR}}$, obtained as $r_i \cdot F_{\text{D-G}}$ (Fig. 2.1). A very high correlation between $F_{\text{D-HR}}$ and $F_{\text{D-G-HR}}$ was found, with almost all $F_{\text{D-HR}}$ values being larger than the $F_{\text{D-G-HR}}$ values, thereby indicating the tendency of the HR method to overestimate F_{D} (Fig. 2.10). When the HR method was applied to the Japanese cedar trees in the FFPRI nursery, reasonable estimations of F_{D} were obtained by the linear regression: $F_{\text{D-G-HR}} = 0.69\ F_{\text{D-HR}}$, $R^2 = 0.83$. In this study, the wounding width of 0.17 cm was assumed resulting in $B = 1.7283$. $F_{\text{D-HR}}$ can vary depending on B (see Eq. 2.12 and 2.13). There are some possibilities that the actual width of the wounding is smaller than 0.17 cm and the overestimation of the wounding effect on $F_{\text{D-HR}}$ would occur. For future calibrations, directly measurements of the wounding width are required.

2.3.6 *Summary of Sap Flow Calibration for the Three Techniques*

We strongly suggest that the radial and azimuthal variations in F_{D} occur in the cross-section of cut segments (Fig. 2.7). As a consequence, these variations must be measured in order to compare sensor output with the gravimetric values of F_{D}. Although the Nagasaka stem segments showed relatively low coefficients of determination associated with the calibration curves of the TD and HFD methods, any tendencies, that is overestimations or underestimations, were not found (Fig. 2.8a, 2.9a). These results indicate that stand-scale measurements of F_{D} with the TD and HFD methods would be accurate and representative and that no calibrations were required at the Nagasaka site. However, for FFPRI stem segments, the TD and HFD methods underestimated F_{D} by 30% or more (Fig. 2.8a and 2.9b), while for the HR

method at this site, an overestimation of approximately 30% was found (Fig. 2.10). Thus, if no corrections were applied to these stem segments the TD and HFD methods would have underestimated E_T by at least 30% and often more, while the HR method would have resulted in an overestimate of E_T of approximately 30%.

Compared with the TD and HFD techniques, the HR method shows very small tree-to-tree differences in calibration results (Fig. 2.10). HR is the only technique among three methods that is based on the physics of heat dissipation (e.g., Fuchs et al. 2017). Sun et al. (2012) showed that the accuracy of the TD method is not dependent on differences in xylem anatomy of the target tree species (i.e., diffuse-porous, ring-porous, and tracheid). However, Fan et al. (2018) suggest that the point or "discrete" F_D measurements derived using the HR and HFD methods are affected by the differences in both hydraulic conductivity and thermal diffusivity between the earlywood and latewood of pine trees. The tree-to-tree and site-specific differences found in this study are probably caused by the heterogeneity of the xylem anatomy including the spatial distribution of the earlywood and latewood. The precise explanation of the uncertainty of sap flow techniques is still unknown (e.g., Steppe et al. 2010), although site- and species-specific calibrations are likely suitable to obtain the most accurate values of F_D and E_T (e.g., Peters et al. 2018; Flo et al. 2019).

2.4 Future Directions in Calibration Studies for Tipping-Bucket Rain Gauges, Tipping-Bucket Flow Meters, and Sap Flow Techniques

The underestimation of rainfall and/or water inflow by tipping-bucket rain gauges and flow meters, respectively, creates a systematic bias dependent on the intensities of inflow. Fortunately, the establishment of correction curves is relatively straightforward, and the equipment required to generate constant inflow (Fig. 2.2), which is a key part of the calibration system, is relatively easy to construct. It is highly recommended to calibrate tipping-bucket rain gauges and flow meters when used for E_I studies. With the exception of Takahashi et al. (2011), Iida et al. (2012), Iida et al. (2018) and Shimizu et al. (2018), among a few others, relatively few studies have evaluated the effects of applying calibration curves on P, T_f, S_f, and/or E_I. Given the findings of work reviewed in this chapter, the degree of systematic underestimations on T_f and S_f, and uncertainties in E_I caused by tipping-bucket rain gauges and flow meters should be investigated for many types of forest ecosystems. We should note that the biases are larger for higher inflow rates (i.e., heavy rainfall) and over shorter time scales (i.e., hourly scale rather than event scale). Studies examining the intrastorm dynamics of interception processes with tipping-bucket rain gauges and flow meters are especially encouraged to utilize calibration curves (e.g., Iida et al. 2017). If tipping-bucket rain gauges and flow meters are already installed in the field without any established calibration curves, in situ static calibrations are strongly

recommended. If practicable, the tipping-bucket gauges could be returned to the laboratory for dynamic calibrations, or, following Shimizu et al. (2018), a generalized correction equation could be employed for larger flow meters with $c_m \geq 150$–200 mL. If the target equipment is out of the application range of the generalized equation, we argue choosing similar types of gauges from Table 2.1 and estimating the potential degree of underestimation. We believe that researchers should recognize the substantial effects of systematic biases of tipping-bucket rain gauges and flow meters on P, T_f, S_f, and E_I, and hope that all manufacturers will provide more detailed calibration results for users in near future.

The IPCC's Fifth Assessment Report (AR5) predicts that extremely large rainfalls will occur more frequently in mid-latitude and tropical areas (Stocker et al. 2014). In Japan, as elsewhere, disasters can be triggered by the localization of heavy rainfall (Tokyo Climate Center, Japan Meteorological Agency 2018). Valid measurements of rainfall are a fundamental requirement for a more precise understanding of the phenomena of localized heavy rainfall. The total degree of underestimation of a rainfall event is affected by not only the inflow intensity but also total number of tips. As such, parallel measurements of rainfall with a 0.5 mm or less tipping-bucket rain gauge and a 1.0 mm or more gauge at the same location are reasonable path forward, provided that data from the lager tipping-bucket rain gauge is selected for events with extremely high intensity. Tipping-bucket rain gauges which regulate high inflow rates using a siphon system are commercially available (e.g., type TB3, HyQuest Solutions Pty. Ltd., Australia). Shedekar et al. (2016) dynamically calibrated the TB3 and showed that the measurement error decreases and stabilizes with increasing inflow rates. Electronic weighing rain gauges, which store rainwater and weigh its amount with a load cell, are available (e.g., Seibert and Morén 1999). Turner et al. (2019) developed an instrument system to measure the change in the depth of stemflow by ultrasonic rangefinders. Theoretically, weighing and depth-measurement approaches have some advantage over tipping-bucket gauges, especially at higher rainfall intensities due to the lack of a tipping-bucket mechanism. However, very few comparisons of rainfall measurements have been made between gauges with inflow regulated and those that have nonregulated flow. Accordingly, further work could compare the differences to interception loss measurements among various tipping-bucket, weighing, and/or depth-measurement gauge combinations under various climate settings. Regardless, as regions of the world experience higher intensity rainfall events, the importance of gauge-corrected measurements from sound calibration procedures will only increase in the future, especially in water-stressed areas where rainfall regimes are changing.

Spurred by Steppe et al. (2010), a large number of TD calibration studies (e.g., Peters et al. 2018) have reported the underestimation of F_D. Such findings raise the importance of TD sensor calibration to accurately estimate E_T. Accordingly, we highlight the necessity of using stem segments in calibration procedures. We would note that the artificial Q_T can be measured directly for stem segments, but artificial F_D cannot be obtained from the single sensor measurement due to the azimuthal and radial trends in F_D. For TD sensors detecting F_D along a sensor length of 2.0 cm, we recommend using stem segments with a sapwood width of ~2.0 cm and applying

enough TD sensors to take the azimuthal variation into account. On the other hand, HFD and HR methods detect F_D at the certain point of sensors. Thus, careful calculations of F_D at each detecting point are required for HFD and HR calibrations. As adopted in this chapter, the HFD method is relatively advantageous to evaluate the radial trend of F_D over the cross section of segments. To increase the number and quality of calibrations for HFD and HR methods, we make a call for future studies to pinpoint the actual F_D at any given sensor position. In addition, although there are numerous calibration studies, the mechanism causing the uncertainties in sap flow techniques is still unknown and should be clarified.

Despite the existence of numerous laboratory-based TD calibrations existed, the application of calibration equations to living trees in forest settings is very limited, with the notable exception of Steppe et al. (2010). Thus, we make a call for both sap flow sensor calibration studies and their applications to field data in order to improve E_T estimates. Wilson et al. (2001) estimated E using both the watershed water balance and eddy covariance methods and evaluated its three components: E_I, E_T, and E_F (Eq. 2.2). Based on the comparison between E and the sum of E_T, derived using the TD method, computed E_I and measured E_F, they suggest the possibility of E_T being underestimated using TD method. Shimizu et al. (2015), however, reported the sum of the three components correspond well with E obtained from both the water balance and eddy covariance methods. Similar findings were reported by Oishi et al. (2008). Compared with the number of studies whose focus is on calibration for the TD method, only a few studies evaluate how well E corresponds to the sum of its components, including E_T. In particular, no studies have reported the application of TD calibration to improve imbalances between E and the sum of E_I, E_T, and E_F. Based on the laboratory calibrations of the TD method, its future application to actual forests is highly recommended to evaluate E_T correctly and to derive a suitable strategy for the precise understanding of the hydrologic cycle in forested watersheds.

Acknowledgments We wish to thank Akita Forestry Research and Training Center for supporting our studies in the Nagasaka Experimental Watershed. This study was partially supported by the project "Research on adaptation to climate change for forestry and fisheries" founded by the Agriculture, Forestry and Fisheries Research Council, Japan, the Global Environmental Research Coordination System from Ministry of the Environment of Japan, and JSPS KAKENHI Grant Numbers JP21710021, JP26450495, JP18K05714 and JP19K06135. We also wish to recognize the anonymous reviewer as well as editors of this volume, especially DE Carlyle-Moses and DF Levia whose comments greatly improved this chapter.

References

Bosch JM, Hewlett JD (1982) A review of catchment experiments to determine the effect of vegetation changes on water yield and evapotranspiration. J Hydrol 55:3–23. https://doi.org/10.1016/0022-1694(82)90117-2

Bosch DD, Marshall LK, Teskey R (2014) Forest transpiration from sap flux density measurements in a southeastern coastal plain riparian buffer system. Agric For Meteorol 187:72–82. https://doi.org/10.1016/j.agrformet.2013.12.002

Burgess SSO, Adams MA, Turner NC, Beverly CR, Ong CK, Khan AA et al (2001) An improved heat pulse method to measure low and reverse rates of sap flow in woody plants. Tree Physiol 21:589–598. https://doi.org/10.1093/treephys/21.9.589

Bush SE, Hultine KR, Sperry JS, Ehleringer JR (2010) Calibration of thermal dissipation sap flow probes for ring-and diffuse-porous trees. Tree Physiol 30:1545–1554. https://doi.org/10.1093/treephys/tpq096

Carlyle-Moses DE, Gash JHC (2011) Rainfall interception loss by forest canopies. In: Levia DF, Carlyle-Moses DE, Tanaka T (eds) Forest ecology and biogeochemistry: synthesis of past research and future directions, ecol studies 216. Springer, Dordrecht, pp 407–423. https://doi.org/10.1007/978-94-007-1363-5_20

Carlyle-Moses DE, Lishman CE (2015) Temporal persistence of throughfall heterogeneity below and between the canopies of juvenile lodgepole pine (Pinus contorta). Hydrol Process 29:4051–4067. https://doi.org/10.1002/hyp.10494

Carlyle-Moses DE, Laureano JF, Price AG (2004) Throughfall and throughfall spatial variability in Madrean oak forest communities of northeastern Mexico. J Hydrol 297:124–135. https://doi.org/10.1016/j.jhydrol.2004.04.007

Carlyle-Moses DE, Lishman CE, McKee AJ (2014) A preliminary evaluation of throughfall sampling techniques in a mature coniferous forest. J For Res 25:407–413. https://doi.org/10.1007/s11676-014-0468-8

Carlyle-Moses DE, Iida S, Germer S, Llorens P, Michalzik B, Nanko K et al (2018) Expressing stemflow commensurate with its ecohydrological importance. Adv Water Resour 121:472–479. https://doi.org/10.1016/j.advwatres.2018.08.015

Clearwater MJ, Meinzer FC, Andrade JL, Goldstein G, Holbrook NM (1999) Potential errors in measurement of nonuniform sap flow using heat dissipation probes. Tree Physiol 19:681–687. https://doi.org/10.1093/treephys/19.10.681

Dunlap F (1912) The specific heat of wood. USDA Forest Service Bulletin No. 110, p 28

Edwards WRN, Warwick NWM (1984) Transpiration from a kiwifruit vine as estimated by the heat pulse technique and the penman-Monteith equation. New Zealand J Agric Res 27:537–543. https://doi.org/10.1080/00288233.1984.10418016

Edwards IJ, Jackson WD, Fleming PM (1974) Tipping bucket gauges for measuring runoff from experimental plots. Agric Meteorol 13:189–201. https://doi.org/10.1016/0002-1571(74)90046-6

Fan J, Guyot A, Ostergaard KT, Lockington DA (2018) Effects of earlywood and latewood on sap flux density-based transpiration estimates in conifers. Agric Meteorol 249:264–274. https://doi.org/10.1016/j.agrformet.2017.11.006

Flo V, Martinez-Vilalta J, Steppe K, Schuldt B, Poyatos R (2019) A synthesis of bias and uncertainty in sap flow methods. Agric For Meteorol 271:362–374. https://doi.org/10.1016/j.agrformet.2019.03.012

Friesen J, Van Beek C, Selker J, Savenije HHG, Van de Giesen N (2008) Tree rainfall interception measured by stem compression. Water Resour Res 44:W00D15. https://doi.org/10.1029/2008WR007074

Fuchs S, Leuschner C, Link R, Coners H, Schuldt B (2017) Calibration and comparison of thermal dissipation, heat ratio and heat field deformation sap flow probes for diffuse-porous trees. Agric Meteorol 244:151–161. https://doi.org/10.1016/j.agrformet.2017.04.003

Fujiwara K, Yamashita K, Hirakawa Y (2004) Mean basic density and density variation within individual trees in major plantation species. Bull FFPRI 3:341–348. (in Japanese with English abstract)

Granier A (1985) Une nouvelle méthod pour la mesure du flux de sève brute dans le tronc des arbres. Ann Sci For 42:193–200. https://doi.org/10.1051/forest:19850204. [Granier A (1985) A new method of sap flow measurement in tree trunks. English translation by Gash JHC, Granier A (2007) In Evaporation, Benchmark Papers in Hydrology 2. Gash JHC, Shuttleworth, WJ (eds). IAHS Press: Oxfordshire; 61–63.]

Helvey JD, Patric JH (1965) Canopy and litter interception of rainfall by hardwoods of eastern United States. Water Resour Res 1:193–206. https://doi.org/10.1029/WR001i002p00193

Herbst M, Roberts JM, Rosier PT, Gowing DJ (2007) Seasonal and interannual variability of canopy transpiration of a hedgerow in southern England. Tree Physiol 27:321–333. https://doi.org/10.1093/treephys/27.3.321

Herwitz SR (1985) Interception storage capacities of tropical rainforest canopy trees. J Hydrol 77:237–252. https://doi.org/10.1016/0022-1694(85)90209-4

Hubbard RM, Stape J, Ryan MG, Almeida AC, Rojas J (2010) Effects of irrigation on water use and water use efficiency in two fast growing Eucalyptus plantations. For Ecol Manag 259:1714–1721. https://doi.org/10.1016/j.foreco.2009.10.028

Iida S (2009) Rainfall redistribution by vegetation. In: Sugita M, Tanaka T (eds) Hydrologic laboratory of the university of Tsukuba, Japan hydrologic science. Kyoritsushuppan, Tokyo, pp 103–117. (in Japanese)

Iida S, Tanaka T (2010) Effect of the span length of Granier-type thermal dissipation probes on sap flux density measurements. Ann For Sci 67:408. https://doi.org/10.1051/forest/2009128

Iida S, Shimizu T, Kabeya N, Nobuhiro T, Tamai K, Shimizu A et al (2012) Calibration of tipping-bucket flow meters and rain gauges to measure gross rainfall, throughfall, and stemflow applied to data from a Japanese temperate coniferous forest and a Cambodian tropical deciduous forest. Hydrol Process 26:2445–2454. https://doi.org/10.1002/hyp.9462

Iida S, Levia DF, Shimizu A, Shimizu T, Tamai K, Nobuhiro T et al (2017) Intrastorm scale rainfall interception dynamics in a mature coniferous forest stand. J Hydrol 548:770–783. https://doi.org/10.1016/j.jhydrol.2017.03.009

Iida S, Levia DF, Nanko K, Sun X, Shimizu T, Tamai K et al (2018) Correction of canopy interception loss measurements in temperate forests: a comparison of necessary adjustments among three different rain gauges based on a dynamic calibration procedure. J Hydrometeorol 19:547–553. https://doi.org/10.1175/JHM-D-17-0124.1

Kimmins JP (1973) Some statistical aspects of sampling throughfall precipitation in nutrient cycling studies in British Columbian coastal forests. Ecology 54:1008–1019. https://doi.org/10.2307/1935567

Kumagai T, Aoki S, Nagasawa H, Mabuchi T, Kubota K, Inoue S et al (2005a) Effects of tree-to-tree and radial variations on sap flow estimates of transpiration in Japanese cedar. Agric Forest Meteorol 135:110–116. https://doi.org/10.1016/j.agrformet.2005.11.007

Kumagai T, Nagasawa H, Mabuchi T, Ohsaki S, Kubota K, Kogi K et al (2005b) Sources of error in estimating stand transpiration using allometric relationships between stem diameter and sap-wood area for *Cryptomeria japonica* and *Chamaecyparis obtusa*. For Ecol Manag 206:191–195. https://doi.org/10.1016/j.foreco.2004.10.066

Kumagai T, Tateishi M, Shimizu T, Otsuki K (2008) Transpiration and canopy conductance at two slope positions in a Japanese cedar forest watershed. Agric Forest Meteorol 148:1444–1455. https://doi.org/10.1016/j.agrformet.2008.04.010

Kumagai T, Tateishi M, Miyazawa Y, Kobayashi M, Yoshifuji N, Komatsu H et al (2014) Estimation of annual forest evapotranspiration from a coniferous plantation watershed in Japan (1): water use components in Japanese cedar stands. J Hydrol 508:66–76. https://doi.org/10.1016/j.jhydrol.2013.10.047

Levia DF, Germer S (2015) A review of stemflow generation dynamics and stemflow-environment interactions in forests and shrublands. Rev Geophys 53:673–714. https://doi.org/10.1002/2015RG000479

Lloyd CR, Marques ADO (1988) Spatial variability of throughfall and stemflow measurements in Amazonian rainforest. Agric Forest Meteorol 42:63–73. https://doi.org/10.1016/0168-1923(88)90067-6

Lopez JG, Licata J, Pypker T, Asbjornsen H (In press) Effects of heater wattage on sap flux density estimates using an improved tree-cut experiment. Tree Physiol. https://doi.org/10.1093/treephys/tpy137

Lu P, Chacko E (1998) Evaluation of Granier's sap flux sensor in young mango trees. Agronomie 18:461–471. https://doi.org/10.1051/agro:19980703

Marshall DC (1958) Measurement of sap flow in conifers by heat transport. Plant Physiol 33:385–396. https://doi.org/10.1104/pp.33.6.385

McCulloh KA, Winter K, Meinzer FC, Garcia M, Aranda J, Lachenbruch B (2007) A comparison of daily water use estimates derived from constant-heat sap-flow probe values and gravimetric measurements in pot-grown saplings. Tree Physiol 27:1355–1360. https://doi.org/10.1093/treephys/27.9.1355

Nadezhdina N, Vandegehuchte MW, Steppe K (2012) Sap flux density measurements based on the heat field deformation method. Trees 26:1439–1448. https://doi.org/10.1007/s00468-012-0718-3

Oishi AC, Oren R, Stoy PC (2008) Estimating components of forest evapotranspiration: a footprint approach for scaling sap flux measurements. Agric Forest Meteorol 148:1719–1732. https://doi.org/10.1016/j.agrformet.2008.06.013

Oki T, Kanae S (2006) Global hydrological cycles and world water resources. Science 313:1068–1072. https://doi.org/10.1126/science.1128845

Ouyang S, Xiao K, Zhao Z, Xiang W, Xu C, Lei P et al (2018) Stand transpiration estimates from recalibrated parameters for the granier equation in a Chinese fir (*Cunninghamia lanceolata*) plantation in southern China. Forests 9:162. https://doi.org/10.3390/f9040162

Peters RL, Fonti P, Frank DC, Poyatos R, Pappas C, Kahmen A et al (2018) Quantification of uncertainties in conifer sap flow measured with the thermal dissipation method. New Phytol 219:1283–1299. https://doi.org/10.1111/nph.15241

Puckett LJ (1991) Spatial variability and collector requirements for sampling throughfall volume and chemistry under a mixed-hardwood canopy. Can J For Res 21:1581–1588. https://doi.org/10.1139/x91-220

Reid LM, Lewis J (2009) Rates, timing, and mechanisms of rainfall interception loss in a coastal redwood forest. J Hydrol 375:459–470. https://doi.org/10.1016/j.jhydrol.2009.06.048

Roth BE, Slatton KC, Cohen MJ (2007) On the potential for high-resolution lidar to improve rainfall interception estimates in forest ecosystems. Front Ecol Environ 5:421–428. https://doi.org/10.1890/060119.1

Schmidt-Walter P, Richter F, Herbst M, Schuldt B, Lamersdorf NP (2014) Transpiration and water use strategies of a young and a full-grown short rotation coppice differing in canopy cover and leaf area. Agric For Meteorol 195:165–178. https://doi.org/10.1016/j.agrformet.2014.05.006

Seibert J, Morén AS (1999) Reducing systematic errors in rainfall measurements using a new type of gauge. Agric For Meteorol 98:341–348. https://doi.org/10.1016/S0168-1923(99)00107-0

Shedekar VS, King KW, Fausey NR, Soboyejo AB, Harmel RD, Brown LC (2016) Assessment of measurement errors and dynamic calibration methods for three different tipping bucket rain gauges. Atmos Res 178:445–458. https://doi.org/10.1016/j.atmosres.2016.04.016

Shimizu T, Kumagai T, Kobayashi M, Tamai K, Iida S, Kabeya N et al (2015) Estimation of annual forest evapotranspiration from a coniferous plantation watershed in Japan (2): comparison of eddy covariance, water budget and sap-flow plus interception loss. J Hydrol 522:250–264. https://doi.org/10.1016/j.jhydrol.2014.12.021

Shimizu T, Kobayashi M, Iida S, Levia DF (2018) A generalized correction equation for large tipping-bucket flow meters for use in hydrological applications. J Hydrol 563:1051–1056. https://doi.org/10.1016/j.jhydrol.2018.06.036

Shinohara Y, Oda T, Kume T, Iida S, Chiu CW, Katayama A et al (2016) Calibration of granier method for Japanese larch and oak. In: 63rd annual meeting of ecological society of Japan, P2–069 (in Japanese)

Shiraki K, Yamato T (2004) Compensation of tipping-bucket flow meters. J Japan Soc Hydrol Water Resour 17:159–162. https://doi.org/10.3178/jjshwr.17.159. (in Japanese with English abstract)

Shiraki K, Sun J, Kagami S, Nagai K, Yokoyama Y, Koyama Y et al (2018) Accracy of low-cost flow meters for stemflow observation including handmade tipping buckets flow meter. J Japan Soc Hydrol Water Resour 31:380–392. https://doi.org/10.3178/jjshwr.31.380. (in Japanese with English abstract)

Steppe K, DJW DP, Doody TM, Teskey RO (2010) A comparison of sap flux density using thermal dissipation, heat pulse velocity and heat field deformation methods. Agric Forest Meteorol 150:1046–1056. https://doi.org/10.1016/j.agrformet.2010.04.004

Stocker TF, Qin D, Plattner G-K, Tignor M, Allen SK, Boschung J et al (eds) (2014) Climate change 2013: the physical science basis: working group I contribution to the fifth assessment report of the intergovernmental panel on climate change. Cambridge University Press, Cambridge/New York, p 1535

Su L, Zhao C, Xu W, Xie Z (2016) Modelling interception loss using the revised gash model: a case study in a mixed evergreen and deciduous broadleaved forest in China. Ecohydrology 9:1580–1589. https://doi.org/10.1002/eco.1749

Sun H, Aubrey DP, Teskey RO (2012) A simple calibration improved the accuracy of the thermal dissipation technique for sap flow measurements in juvenile trees of six species. Trees 26:631–640. https://doi.org/10.1007/s00468-011-0631-1

Swanson RH, Whitfield DWA (1981) A numerical analysis of heat pulse velocity theory and practice. J Exp Bot 32:221–239. https://doi.org/10.1093/jxb/32.1.221

Takahashi M, Giambelluca TW, Mudd RG, DeLay JK, Nullet MA, Asner GP (2011) Rainfall partitioning and cloud water interception in native forest and invaded forest in Hawai'i volcanoes National Park. Hydrol Process 25:448–464. https://doi.org/10.1002/hyp.7797

Takeuchi S, Sugio Y, Shinozaki K, Matsushima D, Iida S (2017) Calibration of heat ratio method by direct measurements of transpiration with weighing root-ball method: a study with Acer palmatum Thunb. J Japan Soc Reveg Tech 43:109–114. https://doi.org/10.7211/jjsrt.43.109. (in Japanese with English abstract)

Taneda H, Sperry JS (2008) A case-study of water transport in co-occurring ring-versus diffuse-porous trees: contrasts in water-status, conducting capacity, cavitation and vessel refilling. Tree Physiol 28:1641–1651. https://doi.org/10.1093/treephys/28.11.1641

Tokyo Climate Center, Japan Meteorological Agency (2018) Primary factors behind the heavy rain event of July 2018 and the subsequent heatwave in Japan from Mid-July Onward. https://ds.data.jma.go.jp/tcc/tcc/news/press_20180822.pdf

Turner B, Hill DJ, Carlyle-Moses DE, Rahman M (2019) Low-cost, high-resolution stemflow sensing. J Hydrol 570:62–68. https://doi.org/10.1016/j.jhydrol.2018.12.072

van Dijk AI, Gash JH, van Gorsel E, Blanken PD, Cescatti A, Emmel C et al (2015) Rainfall interception and the coupled surface water and energy balance. Agric Forest Meteorol 214:402–415. https://doi.org/10.1016/j.agrformet.2015.09.006

van Emmerik T, Steele-Dunne S, Hut R, Gentine P, Guerin M, Oliveira RS et al (2017) Measuring tree properties and responses using low-cost accelerometers. Sensors 17:1098. https://doi.org/10.3390/s17051098

Wilson KB, Hanson PJ, Mulholland PJ, Baldocchi DD, Wullschleger SD (2001) A comparison of methods for determining forest evapotranspiration and its components: sap-flow, soil water budget, eddy covariance and catchment water balance. Agric Forest Meteorol 106:153–168. https://doi.org/10.1016/S0168-1923(00)00199-4

Ziegler AD, Giambelluca TW, Nullet MA, Sutherland RA, Tantasarin C, Vogler JB et al (2009) Throughfall in an evergreen-dominated forest stand in northern Thailand: comparison of mobile and stationary methods. Agric Forest Meteorol 149:373–384. https://doi.org/10.1016/j.agrformet.2008.09.002